# Trajectory and Model Studies of Collisions of Highly Excited Methane with Water Using an ab Initio Potential

Riccardo Conte,*,[†] Paul L. Houston,*,[‡,§] and Joel M. Bowman*,[†]

[†]Department of Chemistry and Cherry L. Emerson Center for Scientific Computation, Emory University, Atlanta, Georgia 30322, United States

[‡]School of Chemistry and Biochemistry, Georgia Institute of Technology, Atlanta, Georgia 30332, United States

[§]Department of Chemistry and Chemical Biology, Cornell University, Baker Laboratory, Ithaca, New York 14852, United States

**ABSTRACT:** Quasi-classical trajectory studies have been performed for the collision of internally excited methane with water using an accurate methane−water potential based on a full-dimensional, permutationally invariant analytical representation of energies calculated at a high level of theory. The results suggest that most energy transfer takes place at impact parameters smaller than about 8 Bohr; collisions at higher impact parameters are mostly elastic. Overall, energy transfer is fairly facile, with values for $\langle \Delta E_{\mathrm{down}} \rangle$ and $\langle \Delta E_{\mathrm{up}} \rangle$ approaching almost 2% of the total excitation energy. A classical model previously developed for the collision of internally excited molecules with atoms (Houston, P. L.; Conte, R.; Bowman, J. M. *J. Phys. Chem. A* **2015**, *119*, 4695−4710) has been extended to cover collisions of internally excited molecules with other molecules. For high initial rotational levels, the agreement with the trajectory results is quite good ($R^2 \approx 0.9$), whereas for low initial rotational levels it is only fair ($R^2 \approx 0.7$). Both the model and the trajectories can be characterized by a four-dimensional joint probability distribution, $P(J_{1,f}\Delta E_1,J_{2,f}\Delta E_2)$, where $J_{1,f}$ and $J_{2,f}$ are the final rotational levels of molecules 1 and 2 and $\Delta E_1$ and $\Delta E_2$ are the respective changes in internal energy. A strong anticorrelation between $\Delta E_1$ and $\Delta E_2$ is observed in both the model and trajectory results and can be explained by the model. There is evidence in the trajectory results for a small amount of $V \leftrightarrow V$ energy transfer from the water, which has low internal energy, to the methane, which has substantial internal energy. This observation suggests that $V \leftrightarrow V$ energy transfer in the other direction also occurs.
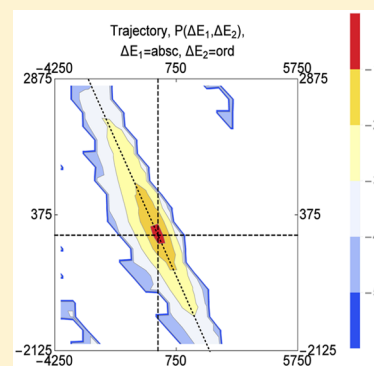
## 1. INTRODUCTION

Many important chemical reactions in combustion chemistry, atmospheric chemistry, and interstellar chemistry take place via the Lindamann mechanism, now nearly a century old:[1,2]

$$A + B \rightleftharpoons A + B^* \quad (k_1/k_{-1}) \tag{R1}$$

$$B^* \rightarrow \text{products} \quad (k_{\mathrm{uni}}) \tag{R2}$$
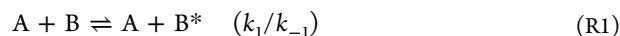
A is typically an atom or small molecule, B is a molecule, and B* is the molecule with vibrational and/or rotational excitation.

We have previously summarized some of the important work on this mechanism,[3−5] and the field has been extensively reviewed elsewhere.[6−12] Thus, only a brief overview will be provided here. Experimental techniques have generated a wealth of data on this process. Some of the more important methods are chemical activation,[13] time-resolved spontaneous infrared fluorescence,[14−16] time-resolved ultraviolet absorption,[17−19] kinetically controlled selective ionization,[20] high-resolution transient IR absorption spectroscopy,[21,22] mass spectroscopy,[23] and time-sliced ion imaging.[24] Theoretical and computational studies have also been informative.[5,11,25−45] In many of the previous experimental and computational studies, the species A in R1 and R2 has been taken as an inert atom. The goal of this work is to investigate a situation in which both A and B are molecules.

The specific choice of B = methane and A = water is motivated in part by previous work on the methane−water potential.[46] The analytical interaction potential is based on a full-dimensional, permutationally invariant analytical representation of energies computed at the CCSD(T)-F12b/haTZ (aug-cc-pVTZ for C and O, cc-pVTZ for H) level of theory. More details concerning the potential and the trajectory calculations are given in Section 2. As noted previously,[46] an understanding of the interaction between methane and water is important to the understanding of methane−water clathrates and also plays a role in gas-phase scattering and combustion chemistry. A second motivation for the methane−water choice is that a direct dynamics investigation of methane−water collisions has recently been reported, albeit with a different level of electronic theory.[32] Jasper et al. investigated energy transfer in the methane as a function of temperature from 300 to 3000 K for collisions with water. However, only 500 trajectories at each of four different temperatures were performed, not enough for a detailed

investigation. Moments of the joint probability distribution (JPD) were reported for the change in methane energy and rotation, though not for similar changes in the water.

A further goal of the current work is to develop a model for energy transfer in collisions between two molecules. The reasons for wanting such a model are two-fold. First, a successful model shows what properties and concepts are most important to the energy transfer process. Second, by delineating what is most important in a particular process, a successful model often suggests computational approximations that can be used to make calculation of the desired results more efficient. The model we develop is based on our previous work for atom−molecule collisions,[3] but here we extend the model to cover molecule−molecule collisions. Details of the model are provided in Section 3. Section 4 presents and summarizes results of the trajectory calculations and of the model. These are discussed in Section 5. A concluding section summarizes our findings and discusses possibilities for future investigation. Table 1 provides a list of acronyms used in the manuscript.

## 2. DESCRIPTION OF METHANE−WATER POTENTIAL AND TRAJECTORY CALCULATIONS

The potential energy surface (PES) employed to simulate collisions of methane with water has been obtained as the sum of

**Table 1. List of Acronyms Used in the Manuscript**

| acronym | meaning |
| --- | --- |
| COM | center of mass |
| JPD | joint probability distribution |
| lhs | left-hand side |
| LOC | line of centers |
| QCT | quasi-classical trajectory |
| rhs | right-hand side |
| TP | turning point |

high-level pre-existing monomer potentials for $CH_4$ and $H_2O$, and a recently reported permutationally invariant two-body $CH_4$−$H_2O$ interaction surface. The flexible, global, full-dimensional and permutationally invariant[47] methane PES was obtained by Warmbier et al.[48] The surface is based on more than 30,000 ab initio RCCSD(T)/aVTZ energies sampled at several $CH_4$ configurations, and it is able to describe dissociation to fragments $CH_3$ + H and $CH_2$ + $H_2$. The water monomer PES employed in this work is the Partridge Schwenke one,[49] based on ab initio energies sampled at the CCSD(T)/aV5Z level. Its analytical form is a modification of Murrell's many-body representation.[50] The PES was empirically adjusted to get spectroscopical accuracy, and properly describes fragmentation to OH + H. Finally, the two-body $CH_4$−$H_2O$ interaction potential[46] was obtained by means of a recently introduced approach,[51] able to design permutationally invariant fitting bases that rigorously describe the zero-interaction asymptotic limit and substantially decrease computational costs of potential calls. This intrinsic two-body potential, called $PES_{2b}$-CSM,[46] has been obtained starting from a database of about 30,000 CCSD(T)-F12b/haTZ ab initio energies. In our previous work,[46] preliminary calculations have shown that the many-body $CH_4$−$H_2O$ PES thus constructed is suitable to simulate collisions involving highly excited methane with water, while even DMC and vibrational calculations for the ground state of the dimer can be accurately undertaken.

Collisional energy transfer has been investigated by running two sets of about 15,000 trajectories starting from highly internally excited $CH_4$. In both cases internal methane excitation was set to 35 410 $cm^{-1}$ (101.24 kcal/mol), close to the dissociation threshold. The starting geometry was chosen to be the equilibrium configuration, while atomic velocities were determined by means of the following procedure. First, we assigned random velocities to atoms. Then, after making $J = 0$, velocities were rescaled to get the desired vibrational energy. Finally, angular velocities were adjusted to get the chosen initial angular momentum $J_{CH_4}$ = 20. Water was started under two different initial conditions. In the first case, the molecule was not rotating and internal excitation was 8637 $cm^{-1}$ (24.69 kcal/mol). In the second simulation, the molecule was prepared with $J_{H_2O} \approx$ 10, and with total internal excitation 18 637 $cm^{-1}$ (53.29 kcal/mol). Since water is an asymmetric rotor, we followed a different approach from the one used for methane in determining initial conditions. We first performed a fully microcanonical sampling by assigning random velocities to water atoms and then rescaled the velocities to match the desired internal excitation. However, in this way, a widespread distribution of initial angular momentum values was produced, so we started a trajectory only when $J_{H_2O}$ was included between 9.9 and 10.1, discarding any other generated initial conditions. In both cases, the initial geometry was the equilibrium one. The two molecules were set 50 au away and given random relative orientation via Euler angle rotation. The impact parameter ($b$) was determined by random and uniform sampling of the variable $(b/b_{max})^2$, and collisional energy was set to 700 $cm^{-1}$ (2 kcal/mol). The maximum impact parameter ($b_{max}$) was chosen to be equal to 13 au upon investigation of average trajectory time and energy transfer at different impact parameter values in a restricted set of preliminary collisions, as described in our previous work.[33] In evolving the dynamics, we employed a time step of 0.1 fs, and each trajectory was stopped either when an unphysical region of the potential was visited (this happened only in about 0.1% of trajectories) or when the two molecules, after the collision, were separated by a distance of at least 20 au. The total energy was typically conserved along trajectories with an accuracy of 1 part in $10^3$ or more, while initial water excitation was large enough to prevent zero-point energy leakage.

## 3. MODEL FOR ENERGY TRANSFER BETWEEN TWO MOLECULES

**Outline of the Model.** The model we develop is applicable to the collision of two molecules in initial rotational levels $J_{1,i}$ and $J_{2,i}$ with initial total (vibrational plus rotational) internal energies $E_{1,i}$ and $E_{2,i}$, respectively. It provides an approximation to the four-dimensional joint probability distribution (JPD) given by $P(J_1, \Delta E_1, J_2, \Delta E_2)$, where $J_1 (\equiv J_{1_f})$ and $J_2 (\equiv J_{2_f})$ are the final rotational levels of molecules 1 and 2, respectively, $\Delta E_1 = E_{1_f} - E_{1,i}$, $\Delta E_2 = E_{2_f} - E_{2,i}$, and $E_{1_f}$ and $E_{2_f}$ are the final internal energies of molecules 1 and 2, respectively.

The model is developed in two stages. First, we use classical mechanics to analyze the motions for two colliding rigid molecules, each in its equilibrium configuration, interacting through a nine-dimensional intermolecular potential $V(\mathbf{R}, \Theta_1, \Theta_2)$, where $\Theta_i = \{\chi_i, \theta_i, \phi_i\}$, [$i = 1,2$], and where $\mathbf{R} = \{x, y, z\}$ is the position of the center of mass (COM) of molecule 2 relative that of molecule 1 located at $\mathbf{R} = \{0,0,0\}$. Turning points (TPs) are then determined for random orientations over the angles $\Theta_1, \Theta_2$ for molecules 1 and 2 and for initial impact
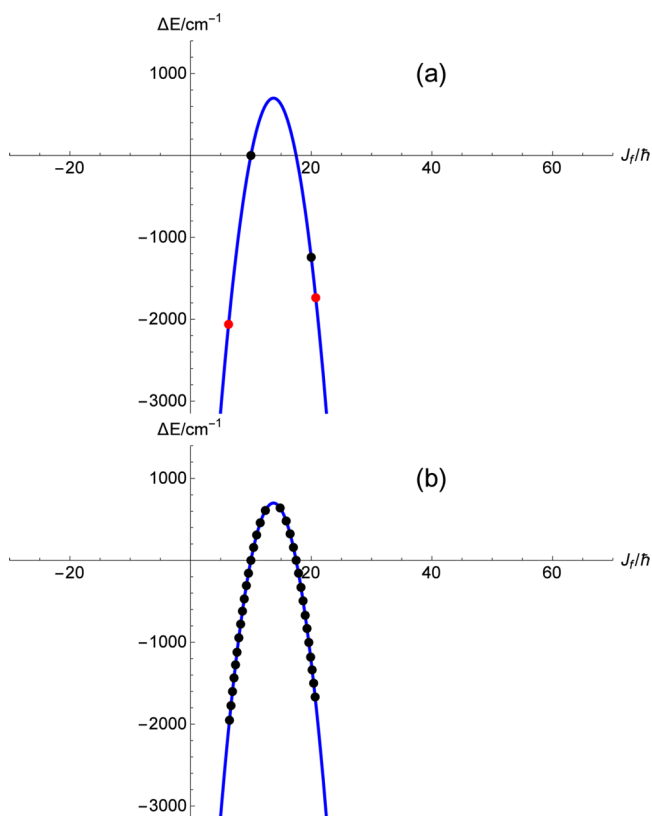
**Figure 1.** (a) Blue curve shows the locus of points for which $\Delta E = \Delta E_1 + \Delta E_2$ is equal to the rhs of eq 7. The black dots show a specific pair of solutions, one of which represents the elastic solution. (b) Every point on the blue curve between the red dots in (a) is also a solution in combination with the elastic solution. In practice, we perform the calculation for a set of points equidistant in $x-y$ space along the blue curve, as shown.

parameters taken between $b_i = 0$ and $b_i = b_{max}$ upon random and uniform sampling of the variable $(b/b_{max})^2$. The turning points are calculated using a straight-line approximation and the intermolecular potential.

An arbitrary unit vector is chosen for the direction of each initial rotational angular momentum, $\mathbf{J_{1,i}}$, of magnitude $J_{1,i}$, and $\mathbf{J_{2,i}}$, of magnitude $J_{2,i}$. When there is rotational energy transfer only, then for each turning point the conservation equations for angular momentum and energy can be solved to find pairs $\{J_{1,f}, J_{2,f}\}$ giving the final rotational states of the molecules, as well to determine each direction relative to the axes of the respective molecule. These directions determine the moments of inertia that are relevant for calculating the associated rotational energy changes $\Delta E_1$ and $\Delta E_2$. The joint probability distribution $P(J_{1,f}, \Delta E_1, J_{2,f}, \Delta E_2)$ is just given by the number of turning points that give these values of the parameters divided by the total number of turning points considered. This stage of the model covers both $R \leftrightarrow T$ and $R \leftrightarrow R$ energy transfer.

In the second stage, we allow the possibility that vibrational energy can be transferred. The model assumes that the probability for the vibrational energy exchange is given by the adiabaticity principle, but that there are also limitations on the amount of vibrational energy that can be transferred depending on the turning point. We calculate the amount of vibrational energy transferred by using Morse potentials to evaluate the degree to which each molecule vibrates. The value of $\Delta E = \Delta E_1 + \Delta E_2$ is then augmented or diminished by the energy change at the turning point due to the vibration of each molecule. In the case when only $V \leftrightarrow T$ transfer is allowed, all of the vibrational energy is used to change $\Delta E$, whereas if $V \leftrightarrow R$ transfer is also allowed, not all of the vibrational energy changes $\Delta E$ because that fraction of it that is transferred to rotation does not change the internal energy of the molecule. The current model neglects $V \leftrightarrow V$ energy transfer.

In summary, the first level of approximation treats the rotational exchange exactly to within classical mechanics and the straight-line trajectory assumption, and it captures much of the physics of the energy transfer. With a second or third level of approximation, there is a broadening of the $\Delta E$ values or both the $\Delta E$ and $J_f$ values due to the vibration of the molecule. This broadening increases the agreement of the model with the results of trajectory calculations. In particular, it allows modeling of the downward energy transfer for systems with $J_i = 0$.

**Details of the Model.** The details of the model for molecule–molecule collisions are an extension of those previously presented for atom–molecule collisions.[3] We calculate the turning point from the intermolecular potential using a straight-line trajectory approximation, a selected impact parameter, and fixed but randomly chosen molecular orientations for each molecule. For trajectories that reach the repulsive region of the potential, the turning point is defined as the point at which the potential is equal to the collision energy, as evaluated from the velocity component in the direction normal to the potential. For straight-line trajectories that do not reach the repulsive region, the turning point is taken as the point on the incoming trajectory, which minimizes the distance along the gradient to the point where $V(R,\Theta_1,\Theta_2) = 0$. This definition conforms most closely to the definition used in the trajectories as the distance of closest approach, although the agreement is only approximate.

Conservation of angular momentum is summarized by the vector equation

$$\mathbf{L_i} + \mathbf{J_{1,i}} + \mathbf{J_{2,i}} = \mathbf{L_f} + \mathbf{J_{1,f}} + \mathbf{J_{2,f}} \tag{1}$$

where the vectors are the initial and final orbital and rotational angular momenta.

Conservation of energy is summarized by the scalar equation

$$E_{i,\text{trans}} + E_{1,i,\text{internal}} + E_{2,i,\text{internal}}$$
$$= E_{f,\text{trans}} + E_{1,f,\text{internal}} + E_{2,f,\text{internal}} \tag{2}$$

or

$$\Delta E = \Delta E_1 + \Delta E_2 = E_{f,\text{internal}} - E_{i,\text{internal}} = -\Delta E_{trans} \tag{3}$$

where $\Delta E$ is the net total change in the internal energy of the two molecules. This change must be equal to the negative of the change in the translational energy of the atom–molecule pair. Let $v_i$ and $v_f$ be the initial and final relative velocities between the two molecules. Because $L_i = \mu v_i b_i$ and $L_f = \mu v_f b_f$, eqs 1 and 2 can be combined by using the initial and final impact parameters $b_i$ and $b_f$:

$$\Delta E = 1/2\mu \left(\frac{L_i}{\mu b_i}\right)^2 - 1/2\mu \left(\frac{L_f}{\mu b_f}\right)^2 \tag{4}$$

where the values in the parentheses are the initial and final relative velocities, respectively. The first term on the rhs of 4 is simply equal to the initial relative energy $E_{rel}$. Thus,

$$\Delta E = E_{\text{rel}} - (1/2)\mu\left(\frac{L_f}{\mu b_f}\right)^2 \tag{5}$$

From eq 1 we see that $L_f$ is the magnitude of $\mathbf{L_i} - \Delta\mathbf{J}$, where $\Delta\mathbf{J} = (\mathbf{J_{1,f}} - \mathbf{J_{1,i}}) + (\mathbf{J_{2,f}} - \mathbf{J_{2,i}})$. Consequently,

$$\Delta E = E_{rel} - (1/2)\mu\left(\frac{\mathbf{L_i} - \Delta\mathbf{J}}{\mu b_f}\right)^2 \tag{6}$$

Although eq 6 gives the solution to the conservation laws that relate $\Delta E$ to $\Delta\mathbf{J}$, it is difficult to use. Typically, although $\mathbf{L_i}$ is known from the initial conditions, $\Delta E$ depends on $\Delta\mathbf{J}$ through both the dependence of rotational energy on $\Delta\mathbf{J}$ and the dependence of the rotational constant on the direction of $\Delta\mathbf{J}$. Additionally, we do not typically know $b_f$. As discussed previously,[3] these problems may be overcome in the straight-line trajectory approximation by separating the incoming and outgoing velocities into judiciously chosen components. Let $\mathbf{v_{rel}}$ be the initial velocity corresponding to $E_{\text{rel}}$. By separating this initial velocity into components normal and tangential to the equipotential contour of $V(\mathbf{R},\mathbf{\Theta_1},\mathbf{\Theta_2})$ at the turning point, we have $\mathbf{v_{rel}} = \mathbf{v_{i,n}} + \mathbf{v_{i,t}}$. Let the energies corresponding to these velocities be $E_n$ and $E_t$. Furthermore, we decompose $\mathbf{v_{i,t}}$ into components perpendicular and parallel to the line of centers (LOC), defined as the line between the COM and the turning point. Then, $\mathbf{v_{i,t}} = \mathbf{v_{i,t,perp}} + \mathbf{v_{i,t,par}}$. Figure 1 of ref 3 is useful in visualizing the relevant vectors.

Now consider the motion along each of these three directions. For incoming motion along the normal, the equipotential contours perpendicular to the motion guarantee that the outgoing motion is also along the normal, so that the directions of $\mathbf{L_{i,n}}$ and $\mathbf{L_{f,n}}$ are along the same line but opposite to one another; thus $\Delta J_n$ must also be along this line. Similarly, motion in the tangential direction perpendicular to the LOC encounters a "hill" or "valley" in the potential. The incoming motion is along a equipotential contour, and to first order, the change in potential is perpendicular to this direction. Thus, the motion remains along the tangential direction as it encounters the potential, where it is reflected back on itself. Again, the directions of $\mathbf{L_{i,t,perp}}$ and $\mathbf{L_{f,t,perp}}$ are along the same line but opposite to one another; thus, $\Delta J_{t,perp}$ must also be along the same line. Motion along the third direction tangential to the normal and parallel to the LOC is unimportant for changes in rotation because the impact parameter is zero.

As we have just seen, for motion along the normal direction and along the tangential direction perpendicular to the LOC, the initial and final trajectories are along the same line, and thus, the initial and final impact parameters are equal. As explained above, the vectors $\mathbf{L_i},\Delta\mathbf{J}$, and $\mathbf{L_f}$ are colinear, so that their vector addition can be replaced by the scalar addition of their magnitudes. For example, along the normal direction, the initial and final impact parameters are equal to the shortest distance between the COM and a line that passes through the turning point and is parallel to the normal (or gradient) to the potential. Let this impact parameter be denoted by $b_n$. Then $L_{i,n} = \mu v_{i,n} b_n$, and $L_{i,n} - \Delta\mathbf{J_n} = L_{i,n} - \Delta J_n$, so that

$$\Delta E = E_n - (1/2)\mu\left(\frac{L_{i,n} - \Delta J_n}{\mu b_n}\right)^2 \tag{7}$$

Because $\Delta J_n = J_{1,f,n} - J_{1,i,n} + J_{2,f,n} - J_{2,i,n}$, there are typically many possible solutions to eq 7. The values of $J_{1,i,n}$ and $J_{2,i,n}$ can be

determined by the following procedure. The magnitudes of the total initial rotational angular momentum, $J_{1,i}$ and $J_{2,i}$, are given by the problem or selected from a rotational temperature. Given, for example, $J_{1,i}$, we choose an arbitrary axis for the initial rotation and project $\mathbf{J_{1,i}}$ onto the direction of $\Delta J_n$ to find $J_{1,i,n}$; a similar procedure is used to find $J_{2,i,n}$. We will then need to average over initial rotational axes as well as over the TPs. The direction for $\Delta J_n$ is determined from the turning point analysis (see below for the calculation of this direction).

Similar equations hold for motion along $\mathbf{v_{t,perp}}$, where $E_n$ is replaced by $E_{t,perp}^{\min}$ and $b_{t,perp}$ is equal to the distance from the COM to the turning point, and for motion along $\mathbf{v_{t,par}}$, where $E_n$ is replaced by $E_{t,par}$ and $b_{t,par} = 0$. In the former case, the combined conservation equation is thus

$$\Delta E = E_{t,\text{perp}}^{\min} - (1/2)\mu\left(\frac{L_{i,t} - \Delta J_t}{\mu b_{t,\text{perp}}}\right)^2 \tag{8}$$

In the latter case, as mentioned earlier, the velocity does not contribute to the angular momentum, i.e., there is an elastic exchange of momenta, and $\Delta J_{t,par}$ is zero. As shown in Figure 2 of ref 4, $E_{t,perp}^{\min}$ is given by the smaller of the values of the potential at the turning point and the value of $E_{t,perp} = (1/2)\mu v_{t,perp}^2$.

For motions along $\mathbf{v_n}$ and along $\mathbf{v_{t,perp}}$, the eqs 7 and 8 can be solved for $J_{1,f,n} + J_{2,f,n}$ and for $J_{1,f,t} + J_{2,f,t}$, respectively. There are, in principle, many combinations of $J_{1,f} + J_{2,f}$ for each equation, but one solution is always the trivial one for which $J_{1,f} = J_{1,i}$ and $J_{2,f} = J_{2,i}$; i.e., for which the collision is elastic.

The directions of all vectors $\mathbf{J_{1,f,n}},\mathbf{J_{2,f,n}},\mathbf{J_{1,f,t}}$, and $\mathbf{J_{2,f,t}}$ are needed to determine the rotational constants, which, for this classical approach, are simply related to the moments of inertia around corresponding rotational vectors. For motion along $\mathbf{v_n}$, the directions of $\Delta\mathbf{J_{1,n}}$ and $\Delta\mathbf{J_{2,n}}$ are given by $\mathbf{v_n} \times \mathbf{b_n}$, where $\mathbf{b_n}$ is a vector of length $b_n$ from the COM to the nearest point on a line through the turning point and parallel to the normal to the potential surface. For motion along $\mathbf{v_{t,perp}}$, the directions of $\Delta\mathbf{J_{1,t,perp}}$ and $\Delta\mathbf{J_{2,t,perp}}$ are given by $\mathbf{v_{t,perp}} \times \mathbf{b_{t,perp}}$, where $\mathbf{b_{t,perp}}$ is a vector of length $b_{t,perp}$ from the COM to the turning point. For many initial $\mathbf{J_i}$ directions, the projection onto $\Delta J_n$ or $\Delta J_{t,perp}$ will be negative. Positive projections correspond to cases where $\mathbf{L_i}$ is in the same direction as the rotation, so that the collision increases $J_i$, whereas negative projections correspond to cases where $\mathbf{L_i}$ is in the opposite direction as the rotation, so that the collision decreases $J_i$. Once $\mathbf{J_f}$ is determined for a particular molecule, the rotational constant may be calculated by determining the moment of inertia of the molecule about its direction and by then converting this moment into a rotational constant. We calculate $\mathbf{J_{1,f}}$ from $\mathbf{J_{1,f}} = \mathbf{J_{1,i}} - (\mathbf{J_{1,i,n}} + \mathbf{J_{1,i,t}}) + (\mathbf{J_{1,f,n}} + \mathbf{J_{1f,t}})$, with a similar equation for $\mathbf{J_{2,f}}$. These steps complete the solution of eq 6, from which we find for each turning point typically several quartets of values $\{J_{1,f},\Delta E_1,J_{2,f},\Delta E_2\}$ that are consistent with conservation of both energy and angular momentum for the situation when only rotational energy change is considered.

An example is helpful in understanding the arguments above. We consider the solution of eq 7 for motion normal to the potential surface. Similar results wre obtained for motion tangential to both the normal and the LOC. Figure 1 provides an example for the case when $J_f = J_{1f} + J_{2f}$ is positive. In this example, $J_{1,i,n} = 20$, $J_{2,i,n} = -10$, $B_{1,n} = 5$ cm$^{-1}$, and $B_{2,n} = 1$ cm$^{-1}$, $b_n = 0.2$ Å, and $L_i = 3.75$. A relatively large value of $L_i$ has been chosen for purposes of illustration. The blue curve shows the locus of points for which $\Delta E = \Delta E_1 + \Delta E_2$ is equal to the rhs of eq

7. The black dots show two possible solutions for the specific case when $J_{1,f,n} = -2J_{2,f,n}$. In this specific case, since $J_{f,n} = J_{1,f,n} + J_{2,f,n}$, we have $J_{f,n} = -J_{2,f,n}$. Thus, the black dot with $\Delta E = 0$ cm$^{-1}$ corresponds to $J_{2,f,n} = -10$ (with $J_{1,f,n} = 20$), whereas the black dot at $\Delta E = -1243$ cm$^{-1}$ corresponds to $J_{2,f,n} = -20$ (with $J_{1,f,n} = 40$). Note that the first black dot is the elastic solution, whereas the second corresponds to a net change in $J_f$ of 10, for which $J_{1,n}$ increased by 20 and $J_{2,n}$ decreased by 10.

There is nothing special about the specific case in (a) for which $J_{1,f,n} = -2J_{2,f,n}$; the factor of $-2$ is arbitrary. In fact, every point on the blue curve between the two red dots is also a solution for some possible pair of $\{J_{1,f,n}, J_{2,f,n}\}$, each in combination with the elastic solution. In practice, we perform the calculation for a set of points equidistant along the blue curve in $x-y$ space, as shown in Figure 1b.

The model to this point is based on angular momentum and energy conservation for two rigid rotor molecules colliding under a realistic potential. Although it can reproduce the trajectory results fairly accurately as we will see later, it cannot account for one important feature. When $J_i = J_{1,i} + J_{2,i}$ is small, there is no probability for energy transfer more negative than the rotational energy corresponding to $J_i$. Specifically, when $J_i$ is zero, there is no probability for any negative value of $\Delta E$ if the molecule is rigid. Trajectories using realistic potentials and allowing the target molecule to change its shape do show probability for negative values of $\Delta E$, even for $J_i = 0$, and it seems intuitive that the reason is that the target molecule is not rigid; it vibrates. As discussed in an earlier paper,[3] one way to look at this is that the energy at the turning point for the equilibrium configuration of the rigid molecule changes as the molecule vibrates. We model the amount of vibrational energy available for the collision as the difference in energy between the turning point energy of the rigid molecule versus the turning point energy of the molecule in a new configuration allowed by vibration. For the level of the model reported here, the treatment is a straightforward extension of that previously considered. Equations 9−12 of the previous paper[3] are applicable here, with the exception that $\Delta E_{vib}$ is now identified as $\Delta E_{1,vib} + \Delta E_{2,vib}$, and the density of states ratio in eq 12 is replaced by the product of ratios, one for $\Delta E_{1,vib}$ and a second for $\Delta E_{2,vib}$. One level of the model includes only $V \leftrightarrow T$ transfer, while a second level also includes $V \leftrightarrow R$ transfer. At this stage, we neglect $V \leftrightarrow V$ transfer between the two molecules. For each molecule, the variation in energy at the turning point is calculated as previously described, either from a simple force field treatment or from trajectories describing the vibrational motion. Computational implementation of the model is similar to that previously described for atom−molecule collisions.[3]

**Computational Implementation of the Model.** The model was implemented using the "PES$_{2b}$-CSM" potential[46] by first calculating 1000 turning points based on 100 randomly selected orientations for the methane and water and, for each orientation set, 10 different impact parameters using the same range of impact parameter as used in the trajectories (13 Bohr). This part of the calculation can be performed in about 150 min using Mathematica on a single processor Macbook Air computer. In a separate calculation, for each set of initial conditions ($J_{i,1}, J_{i,2}, E_{i,1}, E_{i,2}$) and for each impact parameter/orientation set, we calculated solutions to the conservation equations for 1−5 randomly chosen orientations for the original rotational direction of each molecule. These generated typically 140 000−350 000 solutions to the conservation equations that were used to calculate the JPD. This second calculation takes

about 15 min using Mathematica on a single processor Macbook Air computer.

## 4. RESULTS

**Results of the Trajectory Calculations.** The four-dimensional joint probability distribution $P(J_1, \Delta E_1, J_2, \Delta E_2)$, where $J_1 \equiv$
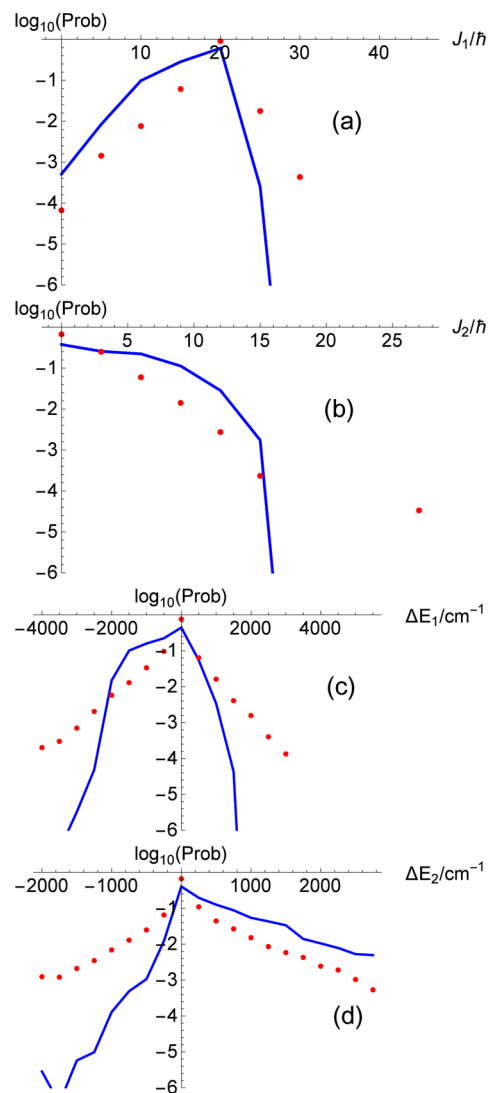


**Figure 2.** One-dimensional projections of the joint probability distribution for trajectories calculated for collisions of methane and water under the conditions described in the text. The initial rotational level of methane is 20, while that of water is 0. The red dots show the projected JPD. (a) $P(J_{1,f})$, (b) $P(J_{2,f})$, (c) $P(\Delta E_1)$, and (d) $P(\Delta E_2)$.

$J_{1,f}$ and $J_2 \equiv J_{2,f}$ is difficult to depict graphically, but there are several projections that are particularly useful. By summing over three of the four variables, we can produce the four one-dimensional projections $P(J_1)$, $P(\Delta E_1)$, $P(J_2)$, and $P(\Delta E_2)$. Alternatively, by summing over two of the four variables, we can produce six two-dimensional projections, of which four are particularly useful: $P(J_1, \Delta E_1)$, $P(J_2, \Delta E_2)$, $P(J_1, J_2)$, and $P(\Delta E_1, \Delta E_2)$. Finally, we can sum $J_1 + J_2$ to form $J$ and $\Delta E_1 + \Delta E_2$ to form $\Delta E$, so as to produce a two-dimensional function most like the atom−molecule JPD: $P(J, \Delta E)$.

Trajectory calculations were performed for methane−water collisions using a collision energy of 700 cm$^{-1}$ with initial internal
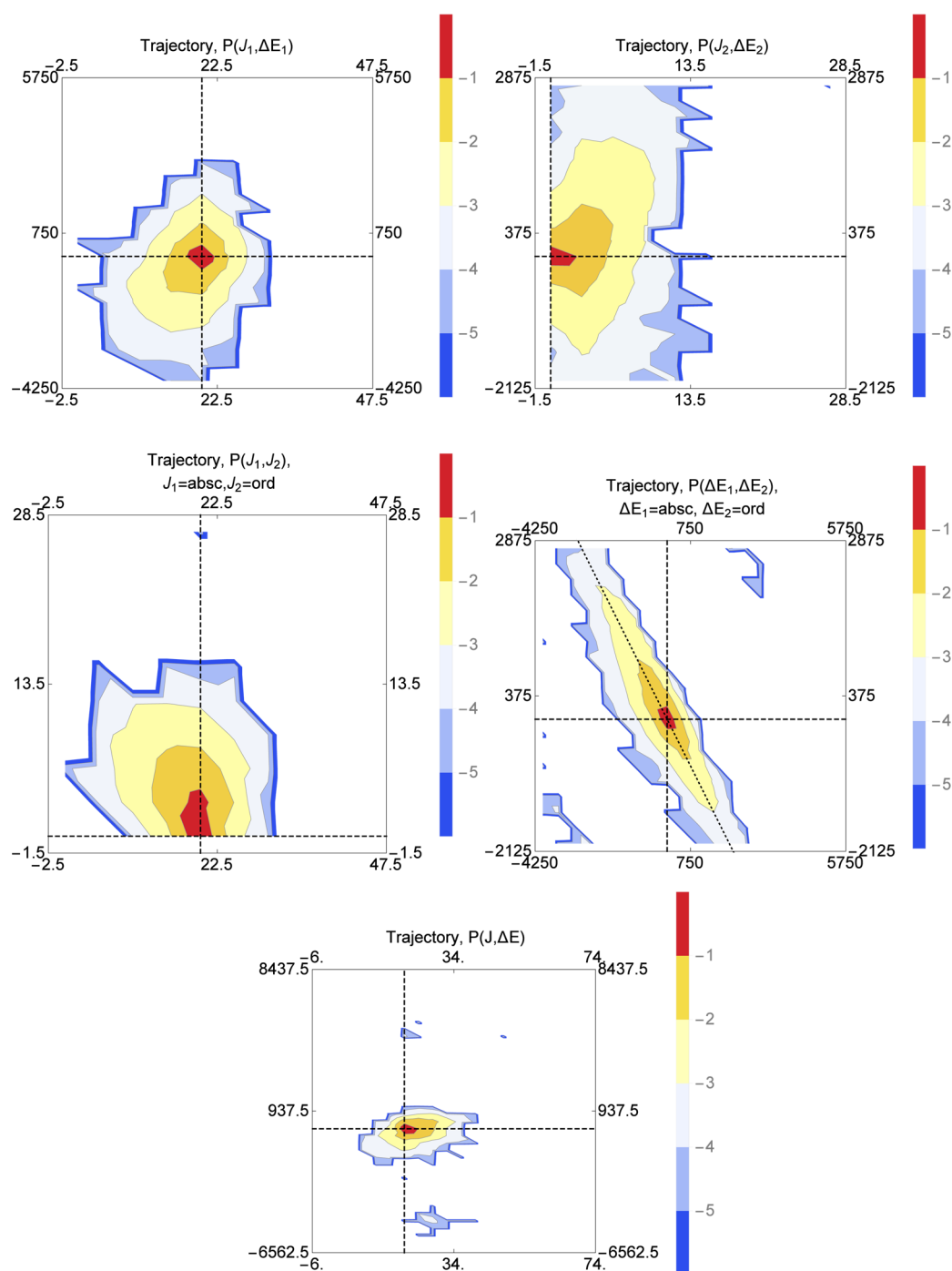
**Figure 3.** Two-dimensional projections of the joint probability distribution for trajectories calculated for collisions of methane and water under the conditions described in the text. The initial rotational level of methane is 20, while that of water is 0. From left to right and top to bottom, the panels show the projections $P(J_{1,f}\Delta E_1)$, $P(J_{2,f}\Delta E_2)$, $P(J_{1,f}J_{2,f})$, $P(\Delta E_1,\Delta E_2)$, and $P(J,\Delta E)$. In each panel, the intersection of the dashed vertical and horizontal lines depicts the elastic condition. The dotted line in the fourth panel shows the condition $\Delta E_1 = -\Delta E_2$. Energy axes are in cm$^{-1}$. The contours represent a log 10 scale of probability and are separated by 1.0 log units.

energies of 35 410 and 8637 cm$^{-1}$, respectively, and with initial rotational levels of 20 and 0 for methane (molecule 1) and water (molecule 2), respectively. One-dimensional projections of the JPD are shown as the red dots in the panels of Figure 2, while two-dimensional projections are shown in Figure 3. The blue curves in Figure 2 will be discussed later.

In order to see how the results might depend on the initial rotational level of the water, trajectory calculations were also performed for methane−water collisions using a collision energy

of 700 cm$^{-1}$ with initial internal energies of 35 410 and 18 637 cm$^{-1}$, respectively, and with initial rotational levels of 20 for methane (molecule 1) and 10 for water (molecule 2). One-dimensional projections of the JPD are shown as the red dots in the panels of Figure 4, while two-dimensional projections are shown in Figure 5. The blue curves in Figure 4 will be discussed later.

In addition to the overall JPD that characterizes the trajectories, we can also gain some insight into the dynamics
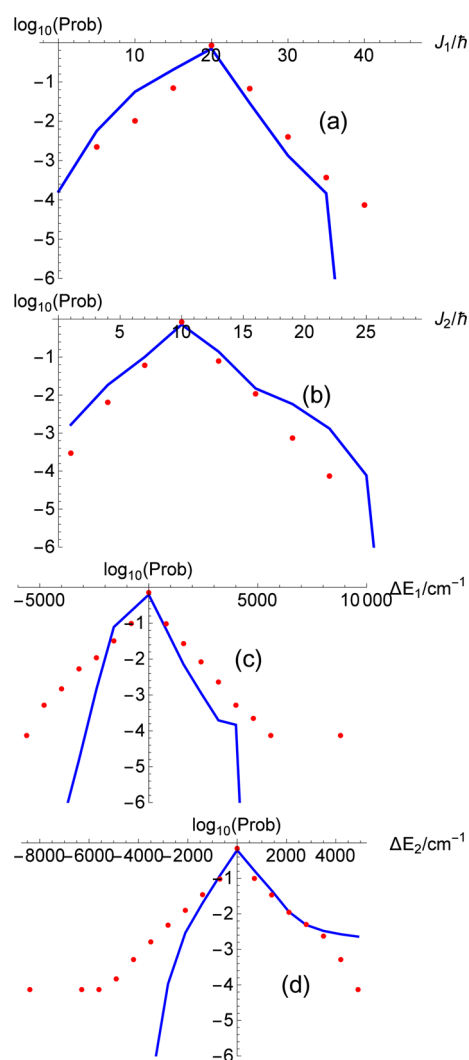
**Figure 4.** One-dimensional projections of the joint probability distribution for trajectories calculated for collisions of methane and water under the conditions described in the text. The initial rotational level of methane is 20, while that of water is 10. The red dots show the projected JPD. (a) $P(J_{1,f})$, (b) $P(J_{2,f})$, (c) $P(\Delta E_1)$, and (d) $P(\Delta E_2)$.

by seeing how various properties depend on the impact parameter. Figure 6 shows a trajectory density plot of, in Figure 6a, the change in internal energy of the methane, and, in Figure 6b, the final rotational level of water. Similar density plots were constructed for $J_{1,f}$, $J_{2,f}$ and $\Delta E_2$ for the initial water rotational level of 10, and for $J_{1,f}$, $\Delta E_1$ and $\Delta E_2$ for the initial water rotational level of 0. Recall that the distribution function from which the impact parameters are chosen increases linearly with the impact parameter. Data such as these can be used to gain insight into how different properties of the methane and water are correlated, as will be explained in Section 5.

**Results of the Model Calculations.** One-dimensional projections of the JPD provided by the model calculations using the same initial parameters as those used in the trajectories for an initial rotational level of water given by $J_{2,i} = 0$ are shown as blue curves in Figure 2. Two-dimensional model projections are shown in Figure 7.

For an initial rotational level of water given by $J_{2,i} = 10$, one-dimensional model projections of the JPD are shown as blue curves in Figure 4, whereas two-dimensional projections are shown in Figure 8.

In all model calculations displayed here, a simple force field method was used to determine how the methane or the water changed internal distances as a result of vibration. This force field method has been described previously.[3] We also ran trajectories to see how the molecular distances varied due to vibration. In either case, these distance variations were used with the known potential energy function to see how the energy at the turning point varied with the vibration of each molecule. This energy is then used to determine the maximum vibrational energy that can be converted to translation.[3] The JPD results using the force field method or the trajectory method were nearly identical.

**Comparison of the Trajectory and Model Calculations.** Two methods were used in order to compare the trajectory and model calculations. In both cases, the trajectory data were used to calculate a JPD using the same energy and rotational binning parameters as used for the model. We used typically 20 bins in the energy range for each of $\Delta E_1$ and $\Delta E_2$, and 10 bins in the range of final rotational levels for each of $J_{1,f}$ and $J_{2,f}$. Thus, there are $20 \times 20 \times 10 \times 10 = 40\,000$ distinct bins in the JPD. The numbers reported below are for inclusion of $R \leftrightarrow T$, $R \leftrightarrow R$, and $V \leftrightarrow T$ energy transfer, except as otherwise noted.

In the first method we simply compared bin-by-bin the values in the normalized trajectory JPD to those in the model JPD and calculated how well the model predicted the trajectory data. The value of $R^2$ for this prediction was 0.73 for an initial water rotational level of $J_{2,i} = 0$ and 0.93 for an initial water rotational level of $J_{2,i} = 10$. This observation is consistent with our model study of atom−molecule collisions,[3] where we found better agreement as the initial rotational level increased.

In the second method, we calculated from each JPD a set of low-order moments: $\langle \Delta E \rangle$, $\langle \Delta E_1 \rangle$, $\langle \Delta E_2 \rangle$, $\langle \Delta E_{\text{down}} \rangle$, $\langle \Delta E_{1,\text{down}} \rangle$, $\langle \Delta E_{2,\text{down}} \rangle$, $\langle \Delta E_{\text{up}} \rangle$, $\langle \Delta E_{1,\text{up}} \rangle$, $\langle \Delta E_{2,\text{up}} \rangle$, $\Delta E_{\text{rms}}$, $\Delta E_{1,\text{rms}}$, $\Delta E_{2,\text{rms}}$, and $\langle \Delta J \rangle$, $\langle \Delta J_1 \rangle$, $\langle \Delta J_2 \rangle$, $\langle \Delta J_{\text{down}} \rangle$, $\langle \Delta J_{1,\text{down}} \rangle$, $\langle \Delta J_{2,\text{down}} \rangle$, $\langle \Delta J_{\text{up}} \rangle$, $\langle \Delta J_{1,\text{up}} \rangle$, $\langle \Delta J_{2,\text{up}} \rangle$, $\Delta J_{\text{rms}}$, $\Delta J_{1,\text{rms}}$, $\Delta J_{2,\text{rms}}$. These parameters are defined in a similar way as those used previously.[3] We then compared the trajectory values for each set of moments to those predicted by the model. For the set of data using the initial water rotational level of $J_{2,i} = 0$, the $R^2$ value for the energy parameters was 0.69, while that for the rotational parameters was 0.73. For the set of data using the initial water rotational level of $J_{2,i} = 10$, the $R^2$ value for the energy parameters was 0.86, while that for the rotational parameters was 0.94. Values of the moments are listed in Table 2.

We also investigated inclusion of $V \leftrightarrow R$ energy transfer in the model on the comparison results. As noted previously,[3] the program calculating the JPD with the inclusion of $V \leftrightarrow R$ transfer takes about five times as long as that for consideration of only $R \leftrightarrow T$, $R \leftrightarrow R$, and $V \leftrightarrow T$ energy transfer. In the current case, it contributes only very minor improvement, resulting in $R^2$ for {bin-by-bin comparison, energy transfer moments, rotational transfer moments} in the $J_{2,i} = 0$ case of {0.70, 0.71, 0.77} and in the $J_{2,i} = 10$ case of {0.89, 0.93 0.94}.

For the previously studied case of atom−molecule collisions,[3] the general agreement for the moments was about $R^2 \approx 0.9$. Thus, the agreement found for the more complicated system of molecule−molecule collisions is about as good when the initial rotational levels are high, but not as good when the initial rotational levels are near zero.

## 5. DISCUSSION

**Impact Parameter Dependence of Collisional Changes: $E_1 \leftrightarrow E_2$ and $J_1 \leftrightarrow J_2$ Correlations.** Trajectory density plots such those shown in Figure 6 can be used to characterize how
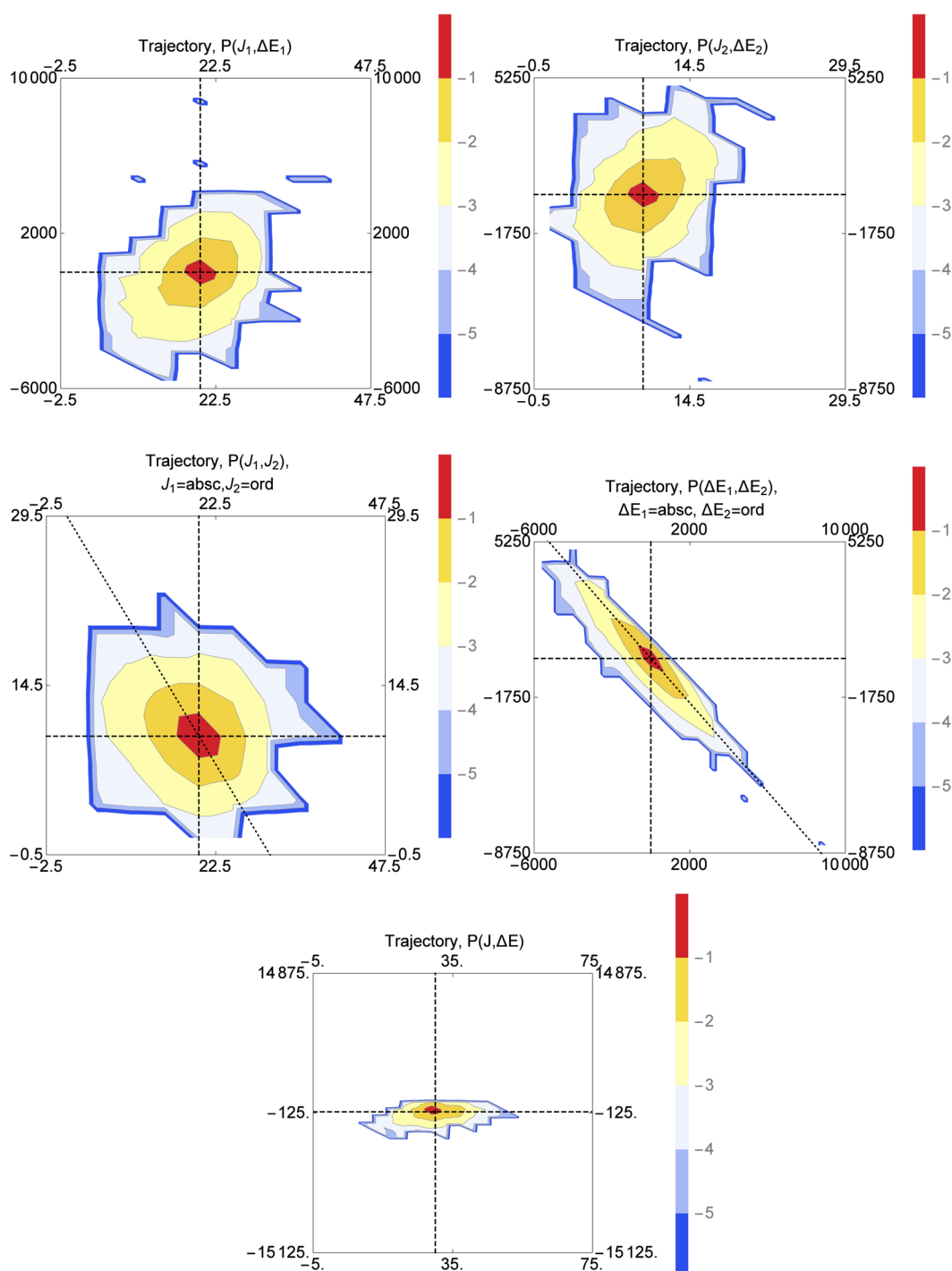
**Figure 5.** Two-dimensional projections of the joint probability distribution for trajectories calculated for collisions of methane and water under the conditions described in the text. The initial rotational level of methane is 20, while that of water is 10. From left to right and top to bottom, the panels show the projections $P(J_{1,f}, \Delta E_1)$, $P(J_{2,f}, \Delta E_2)$, $P(J_{1,f}, J_{2,f})$, $P(\Delta E_1, \Delta E_2)$, and $P(J, \Delta E)$. In each panel, the intersection of the dashed vertical and horizontal lines depicts the elastic condition. The dotted line in the third or fourth panels shows the condition $\Delta J_1 = -\Delta J_2$ or $\Delta E_1 = -\Delta E_2$, respectively. Energy axes are in cm$^{-1}$. The contours represent a log 10 scale of probability and are separated by 1.0 log units.

different properties of the collision depend on impact parameter. Figure 9 shows some examples. The data are for an initial water rotational level of $J_{2,i} = 10$ in Figure 9a,b and $J_{2,i} = 0$ in Figure 9c,d. In Figure 9a,c, the blue and red points show how the absolute values of the internal energy changes for methane and water, respectively, depend on impact parameter. Most of the energy change occurs for impact parameters smaller than 8 Bohr, and $|\Delta E|$ is nearly equal for methane and water, especially for impact

parameters higher than 7 Bohr. Furthermore, one can see that the changes in energy are highly correlated since the sum of the two, $\Delta E = \Delta E_1 + \Delta E_2$ shown by the green points, is close to zero for nearly all impact parameters. Thus, when the internal energy change of one species goes up, that of the other species goes down. This is also evident in the $P(\Delta E_1, \Delta E_2)$ plots in Figures 3 and 5, where the highest probability densities lie along the dotted line of slope $-1$. Note also that the model results of Figures 7 and
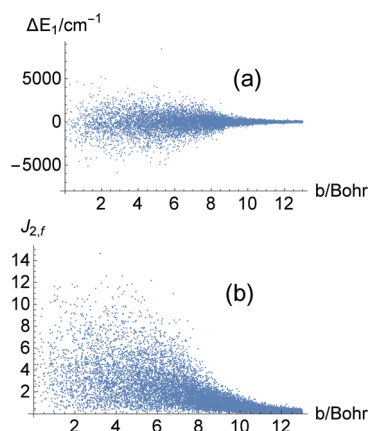
**Figure 6.** Trajectory density plot results for the collision properties as a function of impact parameter. (a) The change in the internal energy of the methane. (b) The final rotational level of water. Both sets of trajectories were for a collision energy of 700 cm$^{-1}$ and an initial methane internal energy of 35 410 cm$^{-1}$. The initial water internal energy was 18 637 cm$^{-1}$ in (a) and 8637 cm$^{-1}$ in (b). The initial rotational state of methane was 20, while that for water was 10 in (a) and 0 in (b).

8 show that the highest probability densities lie along the dotted line of slope −1, although the trend is not quite as strong as for the trajectories.

The reason for the anticorrelation between $\Delta E_1$ and $\Delta E_2$ can clearly be seen in the model; it is a consequence of the conservation equations depicted in Figure 1. Most collisions have a much flatter parabola than shown in the figure, which means that the total $\Delta E = \Delta E_{rot} + \Delta E_{vib}$ is close to zero. Because the probability falls off very strongly with $\Delta E_{vib}$ and less so with $\Delta E_{rot}$, most of the probability density will be along the $\Delta E_{rot} = \Delta E_{rot,1} + \Delta E_{rot,2}$ curve, so that $\Delta E$ will be close to zero energy. If $\Delta E \approx \Delta E_{rot} = \Delta E_{rot,1} + \Delta E_{rot,2} = 0$, it must be that $\Delta E_{rot,1} \approx -\Delta E_{rot,2}$.

In Figure 9b,d, we see the average change in $|\Delta J|$ for methane (blue) and water (red) as a function of impact parameter. The green points give the value of $\Delta J_1 + \Delta J_2$. In Figure 9b, the initial water rotational level is 10, and $\Delta J_1 + \Delta J_2$ is nearly zero, implying that $\Delta J_1$ and $\Delta J_2$ are nearly anticorrelated. Indeed, the $P(J_1, J_2)$ plot of Figures 5 (trajectories) and 8 (model) show a tendency for the maximum probability to lie along the dotted line indicating $\Delta J_1 = -\Delta J_2$. By contrast, in Figure 9d, the initial water rotational level is 0, and $\Delta J_1 + \Delta J_2$ rises commensurately with $|\Delta J_1|$ and $|\Delta J_2|$. The value of $\Delta J_2$ (for water) can only be positive, and the value of $\Delta J_2$ is larger than the value of $\Delta J_1$ (for methane). In this case, the density plots for $P(J_1, J_2)$, shown in Figures 5 and 7, are elongated more along the $J_2$ axis than along the $J_1$ axis.

**$R \leftrightarrow T$ and $R \leftrightarrow R$ vs $V \leftrightarrow T$ Energy Transfer.** A few general trends can be summarized from the trajectory plots of Figures 2−5. From the one-dimensional plots we see that the probability of finding a particular final rotational level has a peak at the initial rotational level and then falls off nearly exponentially for both methane and water. The probability of the rotational energy falls off rapidly though somewhat less steeply than exponentially. From the two-dimensional plots of $J_1$ vs $\Delta E_1$ and $J_2$ vs $\Delta E_2$, we see strong upward curvature in the model plots and somewhat less strong elongation along this direction in the trajectory plots. In general, pure $R \leftrightarrow T$ transfer results in a sharp ridge along the upward rising parabola given for molecule 1 by $\Delta E_1 = E_{rot,1} = (J_{1,f}{}^2 - J_{1,i}{}^2)B_1$, with a similar equation for molecule 2. Model

calculations considering rotation alone give even more sharply peaked ridges than those shown in Figures 3 and 5, which include $V \leftrightarrow T$ energy transfer, so it is clear that vibrational energy is quite important for methane−water energy transfer. The total energy transfer for $J_{2,i} = 0$ is characterized by $\langle \Delta E_{down} \rangle = -802$ and $\langle \Delta E_{up} \rangle = 681$, and for $J_{2,i} = 10$ by $\langle \Delta E_{down} \rangle = -1225$ and $\langle \Delta E_{up} \rangle = 1126$. These values are almost 2% of the total energy, so it would appear that the energy transfer is relatively facile.

A direct comparison between our results and those of Jasper et al.[32] is not possible because different initial conditions were employed in the two studies. Although the initial internal energy of methane was similar, Jasper et al. sampled from temperature distributions at 300, 1000, 2000, and 3000 K, while we have used a microcanonical distribution at a collision energy of 700 cm$^{-1}$. The initial rotational levels for the Jasper et al. work were sampled from the relevant temperature as well, whereas those we used were fixed. Nonetheless, the averaged results are not strikingly different. Our collision energy corresponds to something intermediate between their temperatures of 300 and 1000. For various moments we list the following values (in cm$^{-1}$), where the four numbers listed are for {300 K,[32] 700 cm$^{-1}$($J_{2,i} = 0$)/700 cm$^{-1}$($J_{2,i} = 10$), 1000 K[32]}:

$$\langle \Delta E_{1,down} \rangle = \{-737, -488/-1102, -1265\}$$

$$\langle \Delta E_{1,up} \rangle = \{289, 567/1085, 683\}$$

$$\Delta E_{1,rms} = \{541, 401/704, 813\}$$

$$\langle \Delta J_{1,down} \rangle = \{-3.36, (N/A)/-3.3, -5.56\}$$

$$\langle \Delta J_{1,up} \rangle = \{4.43, 3.9/3.4, 4.29\}$$

$$\Delta J_{1,rms} = \{3.67, 2.5/1.4, 4.33\}$$

**$V \leftrightarrow V$ Energy Transfer.** A somewhat surprising observation is that the trajectory results have probability for $\Delta E_1 > 0$ and $\Delta E_2 < 0$, as shown in the $P(\Delta E_1, \Delta E_2)$ plots of Figures 3 and 5. The latter inequality can only occur when the water gives up vibrational energy to the rotational and/or vibrational excitation of the methane. This transfer, which is somewhat surprising since the methane has so much more internal energy than the water, is more pronounced in the trajectories than in the model. Because $V \leftrightarrow V$ energy transfer has been neglected in the model, the comparison may indicate that this type of energy transfer is important. Future work should focus on how to model such $V \leftrightarrow V$ energy transfer.

Bernshtein and Oref,[52] in their summary of energy transfer conclude that $V \leftrightarrow V$ transfer is the major channel in polyatomic−polyatomic collisions. It is not clear from this study that $V \leftrightarrow V$ transfer is more or less important than $V \leftrightarrow T/R$ transfer, but it is clearly very important. A more extensive comparison between detailed results for polyatomic−polyatomic trajectory studies and the mechanistic conclusions provided in reviews, for example, by Bernshtein and Oref[52] and by Gilbert,[8] is not quite warranted from the result of the current study alone, but as more detailed studies of this kind become available, these conclusions should be revisited.

## 6. SUMMARY AND CONCLUSIONS

QCT calculations have been performed for the collision of internally excited methane with water molecules using an accurate methane−water potential (PES$_{2b}$-CSM)[46] based on a full-dimensional, permutationally invariant analytical representa-
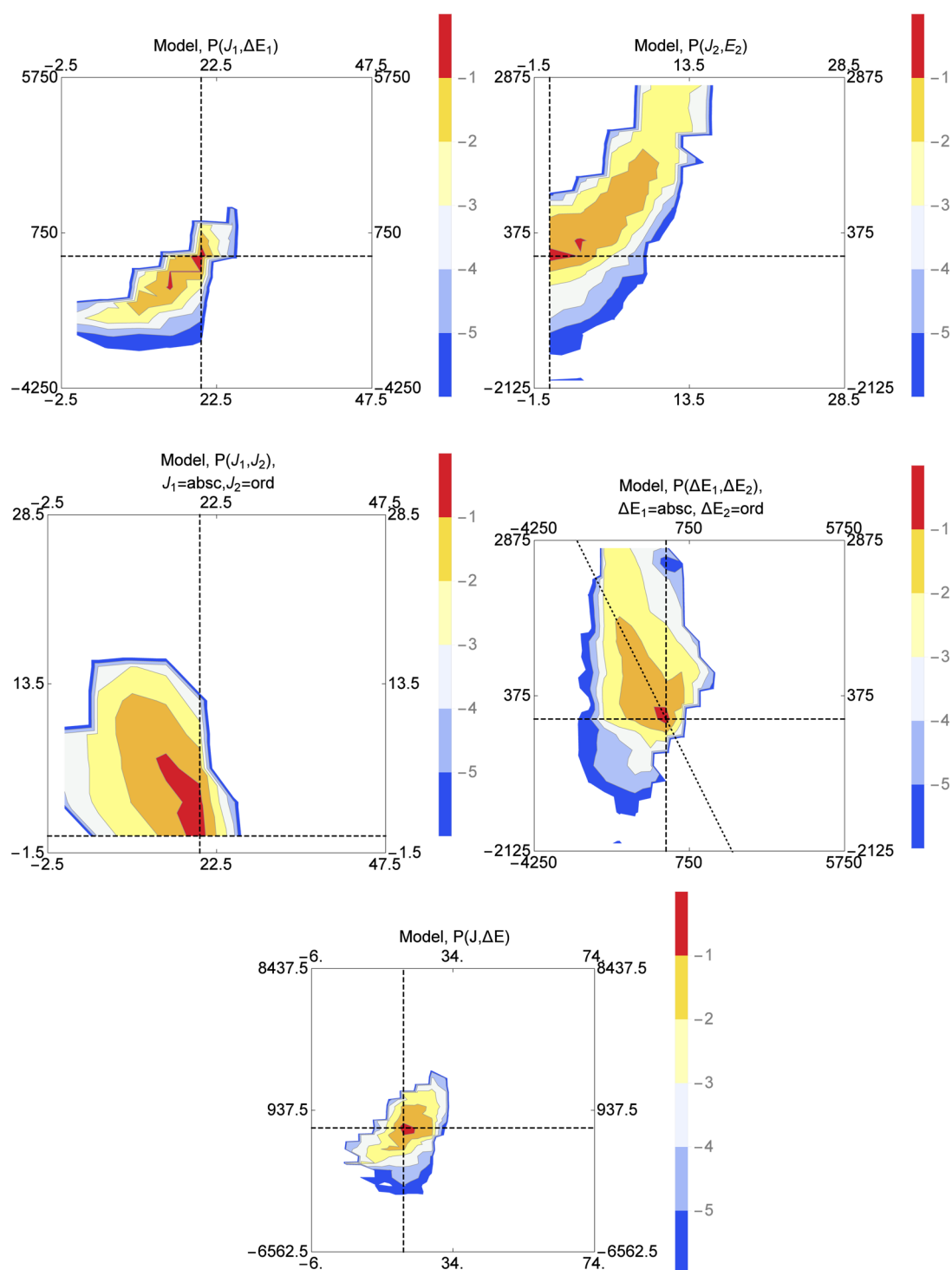
**Figure 7.** Two-dimensional projections of the joint probability distribution for model calculations for collisions of methane and water under the conditions described in the text. The initial rotational level of methane is 20, while that of water is 0. From left to right and top to bottom, the panels show the projections $P(J_{1,f}, \Delta E_1)$, $P(J_{2,f}, \Delta E_2)$, $P(J_{1,f} J_{2,f})$, $P(\Delta E_1, \Delta E_2)$, and $P(J, \Delta E)$. In each panel, the intersection of the dashed vertical and horizontal lines depicts the elastic condition. The dotted line in the fourth panel shows the condition $\Delta E_1 = -\Delta E_2$. Energy axes are in cm$^{-1}$. The contours represent a log 10 scale of probability and are separated by 1.0 log units.

tion of energies calculated at a high level of theory. The potential is important both for understanding methane–water clathrates and for modeling combustion. Trajectory calculations were performed for a collision energy of 700 cm$^{-1}$ and for an initial methane rotational level of $J_{1,i}$ of 20 with an internal energy of 3540 cm$^{-1}$, and for initial water rotational levels of $J_{2,i}$ of 0 and 10 with internal energies of 8637 and 18 637 cm$^{-1}$, respectively.

Examination of the trajectory results indicates that most energy transfer comes from collisions with impact parameters smaller than about 8 Bohr (about 4.2 Å); collisions with larger impact parameters are mostly elastic. Energy transfer is fairly facile; the values of $\langle \Delta E_{down} \rangle$ and $\langle \Delta E_{up} \rangle$ are almost 2% of the total excitation energy.
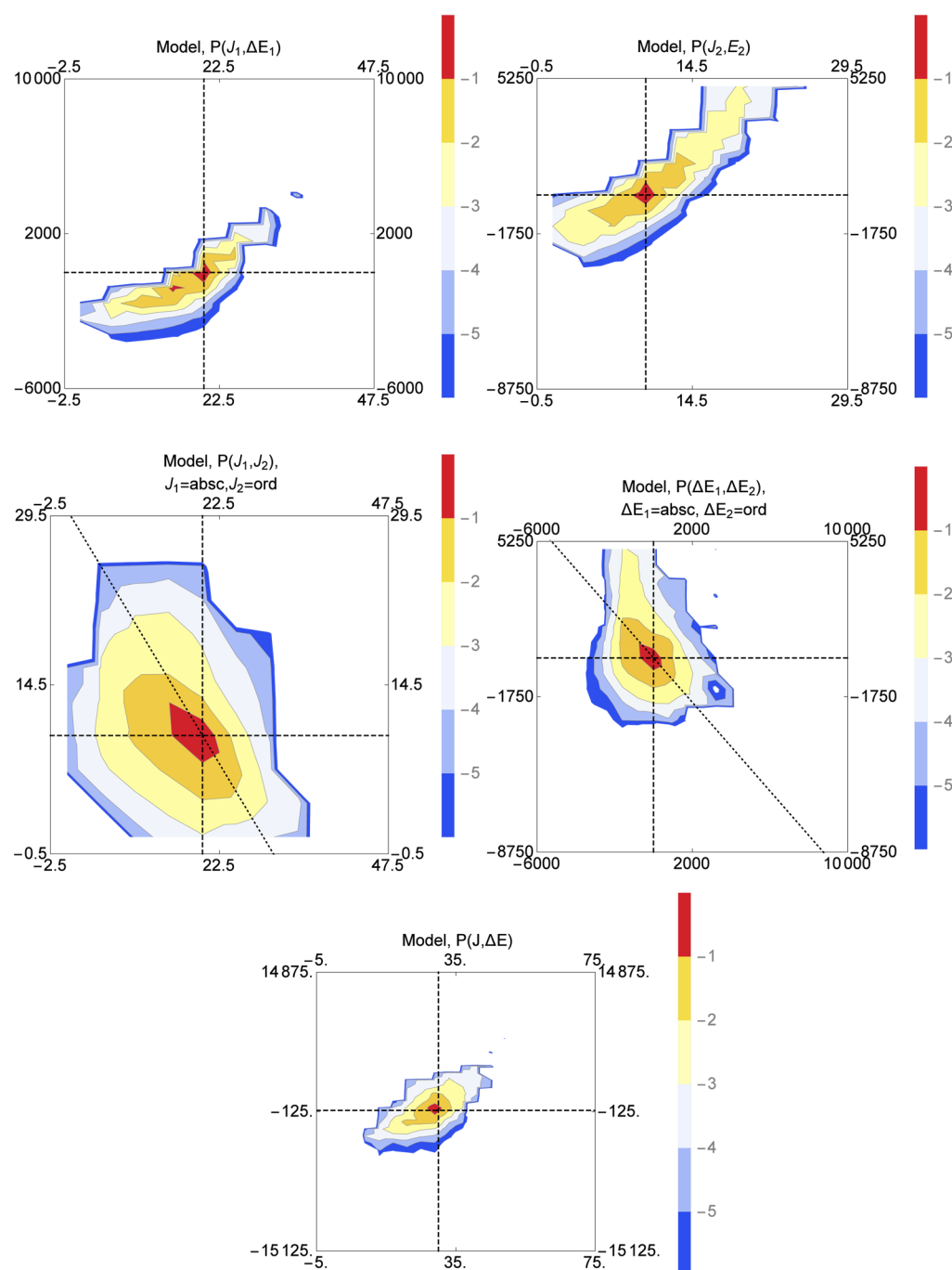
**Figure 8.** Two-dimensional projections of the joint probability distribution for model calculations for collisions of methane and water under the conditions described in the text. The initial rotational level of methane is 20, while that of water is 10. From left to right and top to bottom, the panels show the projections $P(J_{1,f}, \Delta E_1)$, $P(J_{2,f}, \Delta E_2)$, $P(J_{1,f}, J_{2,f})$, $P(\Delta E_1, \Delta E_2)$, and $P(J, \Delta E)$. In each panel, the intersection of the dashed vertical and horizontal lines depicts the elastic condition. The dotted line in the third or fourth panel shows the condition $\Delta J_1 = -\Delta J_2$ or $\Delta E_1 = -\Delta E_2$, respectively. Energy axes are in cm$^{-1}$. The contours represent a log 10 scale of probability and are separated by 1.0 log units.

A classical model for energy transfer has been extended from the atom−molecule collision case[3] to the case for collisions of two molecules. The model explicitly considers $R \leftrightarrow T$, $R \leftrightarrow R$, $V \leftrightarrow T$, and $V \leftrightarrow R$ energy transfer. The inclusion of the first three of these produces good agreement $(R^2 \approx 0.9)$ with the trajectory results for an initial water rotational level of 10 and fair agreement $(R^2 \approx 0.7)$ for an initial water rotational level of 0. Inclusion of $V \leftrightarrow R$ energy transfer results in a very minor improvement in the prediction of the trajectory results, but takes about five times longer for the JPD calculation.

Both the model and the trajectory results show a striking anticorrelation between the internal energy change in methane ($\Delta E_1$) and the internal energy change in water ($\Delta E_2$). The anticorrelation is somewhat stronger in the trajectories than in the model, the latter of which does not include $V \leftrightarrow V$ energy transfer. The anticorrelation in the trajectories is nearly exact for impact parameters larger than about 5 Bohr. From the model, we see that this anticorrelation is due to the fact that for most collisions, particularly those of high impact parameter, the conservation of energy parabola shown in Figure 1 is very

Article

**Table 2. Moments of the Joint Probability Distribution**

| property | model | trajectory | model | trajectory |
|---|---|---|---|---|
| $J_{2,i}$ | 0 | 0 | 10 | 10 |
| $\langle \Delta E \rangle$ | −471 | −63 | −236 | −30 |
| $\langle \Delta E_1 \rangle$ | 390 | 67 | 132 | 0 |
| $\langle \Delta E_2 \rangle$ | −81 | 4 | −104 | −30 |
| $\langle \Delta E_{down} \rangle$ | −933 | −802 | −1016 | −1225 |
| $\langle \Delta E_{1,down} \rangle$ | −1125 | −488 | −830 | −1102 |
| $\langle \Delta E_{2,down} \rangle$ | −556 | −377 | −726 | −417 |
| $\langle \Delta E_{up} \rangle$ | 500 | 681 | 910 | 1126 |
| $\langle \Delta E_{1,up} \rangle$ | 762 | 567 | 1068 | 1085 |
| $\langle \Delta E_{2,up} \rangle$ | 424 | 314 | 930 | 314 |
| $\Delta E_{rms}$ | 736 | 433 | 650 | 724 |
| $\Delta E_{1,rms}$ | 678 | 401 | 716 | 704 |
| $\Delta E_{2,rms}$ | 419 | 251 | 707 | 287 |
| $\langle \Delta J \rangle$ | −2.6 | −0.3 | −1.5 | −0.1 |
| $\langle \Delta J_1 \rangle$ | 3.6 | 1.3 | 0.1 | 0.1 |
| $\langle \Delta J_2 \rangle$ | 1.0 | 1.0 | −1.4 | 0 |
| $\langle \Delta J_{down} \rangle$ | −6.6 | −5.8 | −6.3 | −5.9 |
| $\langle \Delta J_{1,down} \rangle$ | N/A | N/A | −3.5 | −3.3 |
| $\langle \Delta J_{2,down} \rangle$ | −3.1 | −2.9 | −4.5 | −4.5 |
| $\langle \Delta J_{up} \rangle$ | 5.0 | 5.1 | 5.3 | 5.3 |
| $\langle \Delta J_{1,up} \rangle$ | 5.7 | 3.9 | 3.6 | 3.4 |
| $\langle \Delta J_{2,up} \rangle$ | 3.1 | 3.7 | 3.0 | 4.3 |
| $\Delta J_{rms}$ | 4.5 | 1.8 | 3.6 | 2.3 |
| $\Delta J_{1,rms}$ | 5.0 | 2.5 | 2.0 | 1.4 |
| $\Delta J_{2,rms}$ | 3.0 | 2.4 | 3.2 | 2.4 |

shallow, so that the total change of energy is nearly zero despite the possibility that rotational angular momentum levels can change.

The model and the trajectory results also show an anticorrelation between the rotational changes for methane and water when starting in an initial water rotational level of 10, though not when starting in an initial water rotational level of 0. In the latter case, of course, the water rotational level can only increase. The $\Delta J_1 - \Delta J_2$ anticorrelation for the initial water level of 10 is much less strong than the $\Delta E_1 - \Delta E_2$ anticorrelation.

The trajectory data show unambiguously that a small amount of $V \leftrightarrow V$ energy transfer occurs from the water, which has little internal energy, to the methane, which has a large internal energy.

This suggests as well that $V \leftrightarrow V$ energy transfer also occurs in the opposite direction. The model does not include $V \leftrightarrow V$ energy transfer, and future efforts should focus on modeling this type of transfer.

## ■ AUTHOR INFORMATION

**Corresponding Authors**
*E-mail: riccardo.conte@emory.edu.
*E-mail: paul.houston@cos.gatech.edu.
*E-mail: jmbowma@emory.edu.
**Notes**
The authors declare no competing financial interest.

## ■ ACKNOWLEDGMENTS

## ■ REFERENCES

(1) Lindemann, F. A. Discussion on the Radiation Theory of Chemical Action. *Trans. Faraday Soc.* **1922**, *17*, 598−599.

(2) Christiansen, J. A.; Kramers, H. A. Velocity of Chemical Reactions. *Z. Phys. Chem.* **1923**, *104*, 451−471.

(3) Houston, P. L.; Conte, R.; Bowman, J. M. A Model for Energy Transfer in Collisions of Atoms with HighlyExcited Molecules. *J. Phys. Chem. A* **2015**, *119*, 4695−4710.

(4) Houston, P. L.; Conte, R.; Bowman, J. M. Collisional Energy Transfer in Highly Excited Molecules. *J. Phys. Chem. A* **2014**, *118*, 7742−7757.

(5) Conte, R.; Houston, P. L.; Bowman, J. M. Trajectory Study of Energy Transfer and Unimolecular Dissociation of Highly Excited Allyl with Argon. *J. Phys. Chem. A* **2014**, *118*, 7742−7757.

(6) Troe, J. Theory of Thermal Unimolecular Reaction sat Low Pressures. I. Solutions of the Master Equation. *J. Chem. Phys.* **1977**, *66*, 4745−4757.

(7) Troe, J. Theory of Thermal Unimolecular Reactionsat Low Pressures. II. Strong collision rate constants. Applications. *J. Chem. Phys.* **1977**, *66*, 4758−4775L.

(8) Gilbert, R. G. Theory of Collisional Energy Transfer of Highly Excited Molecules. *Int. Rev. Phys. Chem.* **1991**, *10*, 319−347.

(9) Barker, J. R.; Yoder, L. M.; King, K. D. Vibrational Energy Transfer Modeling of Nonequilibrium Polyatomic Reaction Systems. *J. Phys. Chem. A* **2001**, *105*, 796−809.
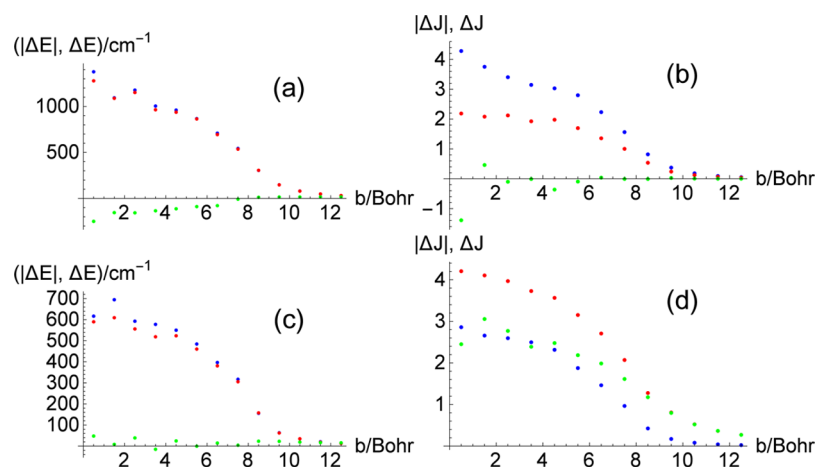
**Figure 9.** Average collision properties for trajectories as a function of impact parameter. (a,c) Variation with impact parameter of $|\Delta E_1|$ (blue), $|\Delta E_2|$ (red), and $\Delta E = \Delta E_1 + \Delta E_2$ (green). (b,d) Variation with impact parameter of $|\Delta J_1|$ (blue), $|\Delta J_2|$ (red), and $\Delta J = \Delta J_1 + \Delta J_2$ (green). The data are for an initial water rotational level of $J_{2,i} = 10$ (a,b) and $J_{2,i} = 0$ (c,d).

(10) Barker, J. R.; Golden, D. M. Master Equation Analysis of Pressure-Dependent Atmospheric Reactions. *Chem. Rev.* **2003**, *103*, 4577−4591.

(11) Barker, J. R.; Weston, R. E., Jr. CollisionalEnergy Transfer Probability Densities P (E, J; E′, J′) for Monatomics Colliding with Large Molecules. *J. Phys. Chem. A* **2010**, *114*, 10619−10633.

(12) Barker, J. R.; Weston, R. E. Correctionto "Collisional Energy Transfer Probability Densities P(E,J;E′, J′)for Monatomics Colliding with Large Molecules. *J. Phys. Chem. A* **2012**, *116*, 799−799.

(13) Tardy, D. C. Competitive Stabilization - New Method for Obtaining Vibrational Energy-Transfer Probabilities in Chemical Activation Systems. *ACS Abstracts* **1977**, *173* (MAR20), 175−175.

(14) Smith, G. P.; Barker, J. R. Energy-TransferRates for Vibrationally Excited Gas-phase Azulene in the Electronic Ground State. *Chem. Phys. Lett.* **1981**, *78*, 253−258.

(15) Barker, J. R. Direct Measurements of Energy-TransferInvolving Large Molecules in the Electronic Ground-State. *J. Phys. Chem.* **1984**, *88*, 11−18.

(16) Barker, J. R.; Toselli, B. M. Infrared-Emission Studies of the Vibrational Deactivation of Benzene Derivatives. *Int. Rev. Phys. Chem.* **1993**, *12*, 305−338.

(17) Hippler, H.; Troe, J.; Wendelken, H. J. Direct Observation of Collisional Deactivation of Highly Excited Toluene. *Chem. Phys. Lett.* **1981**, *84*, 257−259.

(18) Hippler, H.; Lindemann, L.; Troe, J. Collisional Energy Transfer of Vibrationally Highly Excited Molecules. V. UV Absorption Study of Azulene. *J. Chem. Phys.* **1985**, *83*, 3906−3912.

(19) Hippler, H.; Troe, J. Recent Direct Studies of Collisional Energy Transfer on Vibrationally Excited Molecules in the Electronic Ground State. In *Advances in Gas-Phase Photochemistry and Kinetics: Bimolecular Collisions*; Ashfold, M. N. R., Baggott, J. E., Eds.; The Royal Society of Chemistry: London, 1989; p 209.

(20) Hold, U.; Lenzer, T.; Luther, K.; Reihs, K.; Symonds, A. Collisional Energy Transfer Probabilities in the Deactivation of Highly Vibrationally Excited Aromatics. *Ber. Buns. Gesell Phys. Chem.* **1997**, *101*, 552−565.

(21) Wall, M. C.; Mullin, A. S. Supercollision Energy Dependence: State-resolved Energy Transfer in Collisions Between Highly Vibrationally Excited Pyrazine (Evib = 37,900 cm-1 and 40,900 cm-1) and $CO_2$. *J. Chem. Phys.* **1998**, *108*, 9658−9667.

(22) Wall, M. C.; Lemoff, A. S.; Mullin, A. S. Independent Determination of Supercollision Energy Loss Magnitudes and Rates in Highly Vibrationally Excited Pyrazine with Evib = 36,000−41,000 cm-1. *J. Phys. Chem. A* **1998**, *102*, 9101−9105.

(23) Pashutski, A.; Oref, I. Collision-induced Dissociation of Cyclohexadiene by a Vibrationally Hot Collider. *J. Phys. Chem.* **1988**, *92*, 178−182.

(24) Liu, C.-L.; Hsu, H. C.; Lyu, J.-J.; Ni, C.-K. Supercollisions and Energy Transfer of Highly Vibrationally Excited Molecules. *J. Chem. Phys.* **2005**, *123*, 131102.

(25) Brown, N. J.; Miller, J. A. Collisional Energy Transfer in the Low-pressure Limit: Unimolecular Dissociation of $HO_2$. *J. Chem. Phys.* **1984**, *80*, 5568−5580.

(26) Whyte, A. R.; Gilbert, R. G. A Classical Trajectory Calculation of Average Energy Transfer Parameters for the CH3OO + Ar System. *Aust. J. Chem.* **1989**, *42*, 1227−1234.

(27) Lim, K. F.; Gilbert, R. G. Calculation of Collisional-Energy-Transfer Rates in Highly Excited Molecules. *J. Phys. Chem.* **1990**, *94*, 72−77.

(28) Lendvay, G.; Schatz, G. C. Comparison of Master Equation and Trajectory Simulation of the Relaxation of an Ensemble of Highly Vibrationally Excited Molecules. *J. Phys. Chem.* **1994**, *98*, 6530−6536.

(29) Lenzer, T.; Luther, K.; Troe, J.; Gilbert, R. G.; Lim, K. F. Trajectory Simulations of Collisional Energy Transfer in Highly Excited Benzene and Hexafluorobenzene. *J. Chem. Phys.* **1995**, *103*, 626−641.

(30) Jasper, A. W.; Miller, J. A. Collisional Energy Transfer in Unimolecular Reactions: Direct Classical Trajectoriesfor $CH_4 \rightleftarrows CH_3$ + H in Helium. *J. Phys. Chem. A* **2009**, *113*, 5612−5619.

(31) Jasper, A. W.; Miller, J. A. Theoretical Unimolecular Kinetics for $CH_4$ + M $\rightleftarrows$ $CH_3$ + H + M in Eight Baths, M = He, Ne, Ar, Kr, $H_2$,$N_2$, CO, $CH_4$. *J. Phys. Chem. A* **2011**, *115*, 6438−6455.

(32) Jasper, A. W.; Miller, J. A.; Klippenstein, S. J. The Collision Efficiency of Water in the Unimolecular Reaction $CH_4$ (+$H_2O$)→ $CH_3$ + H (+$H_2O$): One-Dimensional and Two-Dimensional Solutions of the Low-Pressure-Limit Master Equation. *J. Phys. Chem. A* **2013**, *117*, 12243−12255.

(33) Conte, R.; Houston, P. L.; Bowman, J. M. Classical Trajectory Study of Energy Transfer in Collisions of Highly Excited Allyl Radical with Argon. *J. Phys. Chem. A* **2013**, *117*, 14028−14041.

(34) Conte, R.; Houston, P. L.; Bowman, J. M. Communication: A Benchmark-Quality, Full-dimensional ab initio Potential Energy Surface for Ar-HOCO. *J. Chem. Phys.* **2014**, *140*, 151101.

(35) Barker, J. R. A State-to-state Statistical-dynamical Theory for Large Molecule Collisional Energy Transfer. *Ber. Bunx. G. Phys. Chem. Chem. Phys.* **1997**, *101*, 566−573.

(36) Nordholm, S.; Freasier, B. C.; Jolly, D. L. Ergodic Collision Theory of Intermolecular Energy Transfer. *Chem. Phys.* **1977**, *25*, 433−449.

(37) Freasier, B. C.; Jolly, D. L.; Nordholm, S. Ergodic Collision Theory of Intermolecular Energy Transfer II. Quantum Effects in the Harmonic Approximation. *Chem. Phys.* **1978**, *32*, 161−168.

(38) Ming, L.; Sewell, T. D.; Nordholm, S. A Simulation Study of Energy Transfer in Methyl Isocyanide-Inert Gas Collisions. *Chem. Phys.* **1995**, *199*, 83−104.

(39) Ming, L.; Davidsson, J.; Nordholm, S. Energy Transfer in Collisions of Small Gas-phase Clusters - Comparison of Molecular Dynamics and Statistical limit Estimates. *Chem. Phys.* **1995**, *201*, 121−140.

(40) Ming, L.; Davidsson, J.; Nordholm, S. Molecular Dynamics Study of Energy Transfer in Binary Collisions of Water Molecules. *J. Chem. Phys.* **1996**, *104*, 9001−9015.

(41) Nilsson, D.; Nordholm, S. Statistical Model of Energy Transfer in Molecular Collisions: De-energization of Highly Excited Toluene. *J. Chem. Phys.* **2002**, *116*, 7040−7048.

(42) Nilsson, D.; Nordholm, S. Modeling Energy Transfer in Molecular Collisions: Statistical Theory versus Experiment for Highly Excited Toluene and Azulene. *J. Chem. Phys.* **2003**, *119*, 11212−11220.

(43) Nilsson, D.; Nordholm, S. Statistical Theory of Collisional Energy Transfer in Molecular Collisions. Trans-Stilbene Deactivation by Argon, Carbon Dioxide, and n-Heptane. *J. Phys. Chem. A* **2006**, *110*, 3289−3296.

(44) Lenzer, T.; Luther, K.; Nilsson, D.; Nordholm, S. PECT Model Analysis and Predictions of Experimental Collisional Energy Transfer Probabilities P(E′,E) and Moments (Delta E) for Azulene and Biphenylene. *J. Phys. Chem. B* **2005**, *109*, 8325−8331.

(45) Jasper, A. W.; Plelzer, K. M.; Miller, J. A.; Karmarchik, E.; Harding, L. B.; Klippenstein, S. J. Predictive a priori Presure-dependent Kinetics. *Science* **2014**, *346*, 1212−1215.

(46) Qu, C.; Conte, R.; Houston, P. L.; Bowman, J. M. "Plug and Play" Full-dimensional ab initio Potential Energy and Dipole Moment Surfaces and Anharmonic Vibrational Analysis for CH4-H2O. *Phys. Chem. Chem. Phys.* **2015**, *17*, 8172−8181.

(47) Braams, B. J.; Bowman, J. M. Permutationally invariant potential energy surfaces in high dimensionality. *Int. Rev. Phys. Chem.* **2009**, *28*, 577−606.

(48) Warmbier, R.; Schneider, R.; Sharma, A. R.; Braams, B. J.; Bowman, J. M.; Hauschildt, P. H. *Ab initio* modeling of molecular IR spectra of astrophysical interest: application to $CH_4$. *Astron. Astrophys.* **2009**, *495*, 655−661.

(49) Partridge, H.; Schwenke, D. W. The determination of an accurate isotope dependent potential energy surface for water from extensive *ab initio* calculations and experimental data. *J. Chem. Phys.* **1997**, *106*, 4618−4639.

(50) Murrell, J. N.; Carter, S.; Farantos, S. C.; Huxley, P.; Varandas, A. J. C. *Molecular Potential Energy Functions*; Wiley: Chichester, 1984.

(51) Conte, R.; Qu, C.; Bowman, J. M. Permutationally-invariant Fitting of Many-body, Non-covalent Interactions with Application

toThree-body Methane-water-water. *J. Chem. Theory Comput.* **2015**, *11*, 1631−1638.

(52) Bernshtein, V.; Oref, I. Collisional Energy Transfer in Polyatomic Molecules in the Gas Phase. *Isr. J. Chem.* **2007**, *47*, 205−214.